FINAL TECHNICAL REPORT

for

NASA Grant NAG-5249

Spectrophotometry of Planets, Asteroids and Satellites from the International Ultraviolet Explorer Satellite

by

M. G. Tomasko, B. Zellner, S. Martinek, and T. Gehrels

Lunar and Planetary Laboratory

University of Arizona

May 1, 1981

SUMMARY

From 1978 to 1980 we received support to observe Jupiter, several types of asteroids, and several solar-type stars with the International Ultraviolet Explorer (I.U.E) satellite. A total of 14 8-hour I.U.E. observing sessions were allocated to this program over a two-year period. These observing sessions were extremely successful and resulted in 39 spectra of 11 asteroids and 9 solar-type stars as well as 57 spectra at various locations on the disk of Jupiter. The Jupiter observations include a total of 5 center-to-limb series of spectra at various latitudes and a North-South series along the central meridian. In the range from 2000-3000 Å the planet shows a striking decrease in brightness at latitudes greater than about 30 degrees, and exhibits limb-brightening at low latitudes and limb-darkening at high latitudes. Preliminary results indicate that about 6 km-amagats of clean hydrogen are required above a haze of absorbing aerosols to reproduce the limb-brightening observed at 2500Å in the equatorial regions. At higher latitudes, the aerosols extend to even higher levels of the atmosphere. Comparison of the Jovian data with detailed model calculations and the analyses of the asteroid spectra are still in progress with other support.

TABLE OF CONTENTS

I. Introduction

This final technical report summarizes our work under NASA Grant NSG-5249 from 1978 to 1980 , involving observations of Jupiter, several asteroids, and some solar-type stars using the International Ultraviolet Explorer (I.U.E.) satellite. In the next section we briefly review the main objectives of our observing program. Section III presents a log of the observations obtained, describes our preliminary data processing, and qualitiatively describes the implications of the data. A final section describes the current state of the detailed analysis and interpretation of the Jovian limb-darkening observations and indicates our plans for further work.

II. Objectives

A. Jupiter

Ultraviolet observations of the albedo of Jupiter in the region between 2000Å and 3000Å made before the launch of IUE limited the abundance of clean gas above a region of absorbing aerosols in Jupiter's atmosphere to be less than 12 km-amagats of hydrogen. Infrared observations indicated the presence of 2 to 3 times this much hydrogen above a cloud layer. One suggestion for resolving this apparent discrepancy involved the presence of fine absorbing dust mixed with the gas above the clouds. If the aerosols were sufficiently small, they could have a large optical depth in the ultraviolet while remaining almost transparent in the infrared.

The IUE satellite offered the first opportunity to measure the center-to-limb variations of selected latitudes on Jupiter in the ultraviolet. Such observations would be sensitive to the presence and vertical distribution of absorbing aerosols mixed with the gas above Jupiter's clouds. If the dark aerosols were mixed to high levels in the atmosphere, the planet would show limb darkening in the ultraviolet. On the other hand, limb brightening would indicate the existence of a relatively clear gaseous region at the top of the atmosphere. The variation of the amount of limb brightening with wavelength in the ultraviolet would constrain the location and optical properties of the aerosols.

B. Asteroids

A second objective of our observing program was to study the minerology of a variety of types of asteroids by extending the existing spectrophotometry of these bodies into the ultraviolet. Asteroids of type S and C, and unclassifiable silicate-rich objects such as 4 Vesta, should show a very deep and wide absorption band in the 0.22-0.36 μm spectral region due to charge-transfer transitions in Fe^{2+} and similar ions. The shape and depth of the band is sensitive to the type of ferrosilicate mineralogy; fine structure is not expected but would be of great interest if detected. For asteroids of type M, believed to consist of relatively pure metal, and type E, believed to consist of relatively pure magnesian silicates, the Fe^{2+} band should be weak or absent. The nature of any UV absorptions found should give good indications of the precise mineralogy present.

For Jupiter and especially for the asteroids the observed spectrum must be divided by that of the sun, which is very irregular and not accurately known in the vacuum ultraviolet. Thus we included in our observing list several stars known from visible spectrophotometry to be good solar analogues.

III. Observations and Preliminary Reductions

A. Log of Observations

A total of 106 images were obtained during 14 observing sessions. Approximately 96 of the images provided useful data including 57 spectra of various locations on Jupiter and 39 spectra of 11 asteroids and 9 solar-type stars. The IUE LWR images are summarized in the following two tables. Table 1 lists the asteroid and star data obtained by image number. Also indicated are the object of each image, aperture used, exposure time and the date of acquisition. Table 2 lists the Jupiter images, date acquired,exposure time, and a brief description of the location of each image on the disk of Jupiter. The Jupiter data were obtained in the long-wavelength low-dispersion mode with the 3 arc-second aperture at exposure times generally of

TABLE 1 ASTEROID AND STAR IMAGE DATA

IMAGE	OBJECT	T	AP	EXP	DATE
1530	Vesta	A	S	720	141/78
1531	Vesta	A	S	3000	"
1532	Vesta	A	S	300	"
1533	12 Victor	A	S	480	"
1538	16 Psycho	A	L	4500	142/78
1539	Pallas	A	S	960	"
1540	Pallas	A	S	4140	"
1540	Pallas	A	L	600	"
1888	16 Cyga	S	S	150	206/78
1888	16 Cyga	S	L	282	"
1889	16 Cyga	S	L	1260	"
1890	Ceres	A	S	600	"
1890	Ceres	A	L	1200	"
1891	10 Hygiea	A	L	4800	
1895	9 Metis	A	L	3000	207/78
1896	3 Juno	A	L	3600	"
1897	HD181655	S	S	198	"
1897	HD181655	S	L	390	"
1907	44 NYSA	A	L	7200	209/78
1908	44 NYSA	A	L	7200	"
6085	HD86728	S	S	120	314/79
6085	HD86728	S	L	300	"
6086	HD45184	S	S	300	315/79
6086	HD45184	S	L	720	"
6087	HD28068	S	L	780	"
6088	HD10800	S	S	180	"
6088	HD10800	S	L	450	"
6089	HD10800	S	S	120	"
6089	HD10800	S	L	1500	"
6484	27 Eute	A	L	3000	362/79
6485	511 Davida	A	L	14400	"
6486	HD191854	S	S	780	363/79
6486	HD191854	S	L	1800	"
6487	3 Juno	A	L	2880	"
6488	HD89010	S	S	200	"
6488	HD89010	S	L	480	"
6489	HD89010	S	S	200	"
6490	HD13974	S	S	72	"
6490	HD13974	S	L	180	"

note:

a.) All images are LWR
b.) Type (T) S : Star, A : Asteroid
c.) Aperture (AP) S : Small, L : Large
d.) Exposure time (EXP) is in seconds
e.) Date : day/year

TABLE 2. JUPITER IMAGE SUMMARY

IMAGE	DATE	EXP	COMMENTS
1399	117/79	5 min	Near disk center, exp. test
1400	"	4 min	" " " " "
1401	"	"	Off disk, tracking test
1402	"	"	" " " "
1406	118/78	4 min	Near Red Spot
1407	"	"	
1408	"	"	W-E center-limb
1409	"	"	scan
1410	"	"	
1411	"	"	Near East limb
3409	7/79	30 min	Near East limb
3410	"	"	
3411	"	"	E-W limb-limb scan
3412	"	"	
3413	"	"	Near West limb
6054	313/79	4 min	Partially on South limb
6055	"	"	South limb
6056	"	"	Off disk, tracking error
6057	"	"	
6058	"	"	S-N limb-limb scan
6059	"	"	
6060	"	"	
6061	"	"	
6062	"	"	
6063	"	"	North limb
6069	314/79	4 min	Near West limb
6070	"	"	
6071	"	"	
6072	"	"	
6073	"	"	W-E Equatorial
6074	"	"	limb-limb scan
6075	"	"	
6076	"	"	
6077	"	"	
6078	"	"	
6079	"	"	East limb
6080	"	"	Partially on East limb
6081	"	"	Just off East limb
6082	314/79	90 sec	Disk center
6083	"	45 sec	" "
6108	316/79	4 min	Tracking error,
6109	"	"	partially on
6110	"	"	North limb
6111	"	10 min	
6112	317/79	4 min	Near North limb
6113	"	"	" " "
6114	"	"	" " "
6115	"	"	" " "
6116	"	"	" " "
6117	"	"	" " "
6118	"	"	
6119	"	"	W-E partial
6120	"	"	mid-latitude
6121	"	"	scan
6122	"	"	
6123	317/79	4 min	West limb
6124	"	"	
6125	"	6 min	
6126	"	"	
6127	"	"	W-E high latitude
6128	"	"	limb-limb scan
6129	"	"	
6130	"	"	
6131	"	"	East limb
6132	"	"	Partially on East limb
6133	"	"	Just off East limb
6134	"	4 min	Off disk, tracking error

Note: All exposures are small aperture, low resolution, long wavelength camera.

several minutes. Two east-west series of 4-minute exposures and one series of 30-minute exposure at equatorial latitudes, one series at high latitude (6-minute exposure each), one series at mid-latitudes (4 minutes each) and a north-south series of exposures (4 minutes each) were obtained by various techniques involving tracking on the Galilean satellites. While somewhat cumbersome, with practice a series of 8 to 12 exposures covering one scan across Jupiter could be obtained by this method in an 8 hour shift. Reliable information concerning pointing required accurate calculation of the positions of the Galilean satellites relative to Jupiter as seen from the IUE orbit -- a task contributed (at no small effort) by Lonny Lane at the Jet Propulsion Laboratory. Positions of the aperture could be offset from the guiding satellite to an accuracy comparable to the size of the 3 arcsecond aperture. However, the direction and rate of motion of the satellites relative to Jupiter is known to very great accuracy. By taking a series of spectra over a period of several hours while continuing to track the same satellite, spectra could be obtained that included the crossing of the limb (see Fig. 7 below), and the locations of the aperture on Jupiter during each exposure in the series could be found to high accuracy.

B. Reductions

The computer processing performed on the IUE image data to enable further scientific analysis can be separated into three distinct levels:

1). Processing common to all images,

2). Separate processing specific to either asteroid and star images or to Jupiter images,

3). Special techniques for extraction of limb darkening from noisy Jovian spectra

The data reduction employed in the first two levels will be briefly described here, while the level three processing will be discussed in Section IV.

A preliminary processing sequence was applied to all the image data supplied on the Guest Observer tapes. This was performed in order to generate a local set of archival and working image data tapes and to provide an initial examination of the data.

All the observed raw LWR image data were processed using the standard IUESIPS schemes for low dispersion single or double aperture exposures. (Some of the asteroid and star observations were double aperture exposures).

Figure 1 illustrates the basic steps of level 1 processing. The first step was the transcription of the GPIS, ESSR, and ESLO (see IUE Image Processing Manual, version 1.0, Table 8-1, page 8-6,7) files onto local archival tapes. The data were reformatted for default capability with the available Control Data Corporation computer. The ESLO, or file 5, data containing the merged extracted spectra for all the Jupiter images were then copied to a working tape to provide easy subsequent access. Separation of Jupiter and asteroid data occurred at this stage.

The file 5 image data were then processed by two routines, CFILE5 and FLUX5. These routines provide an integer list of the contents of the file, (IUE Image Processing Manual, Version 1.0, Table 8-1, page 8-6,7) as well as an IUE flux number (FN) list of the gross, background, and net spectra. This output facilitated the selection of wavelength regions containing usable data with adequate signal-to-noise.

At this stage the asteroid and star data were ready for level 2 processing. The Jupiter spectra went through an additional step in order to remove the instrumental response function. The May 1980 (IUE NASA Newsletter, June 1980) version of the IUE Absolute Calibration for low dispersion images was utilized to remove the instrumental response function from the net spectra of the file 5 data. Application of the 1/S function effectively removes the wavelength dependence of the response and

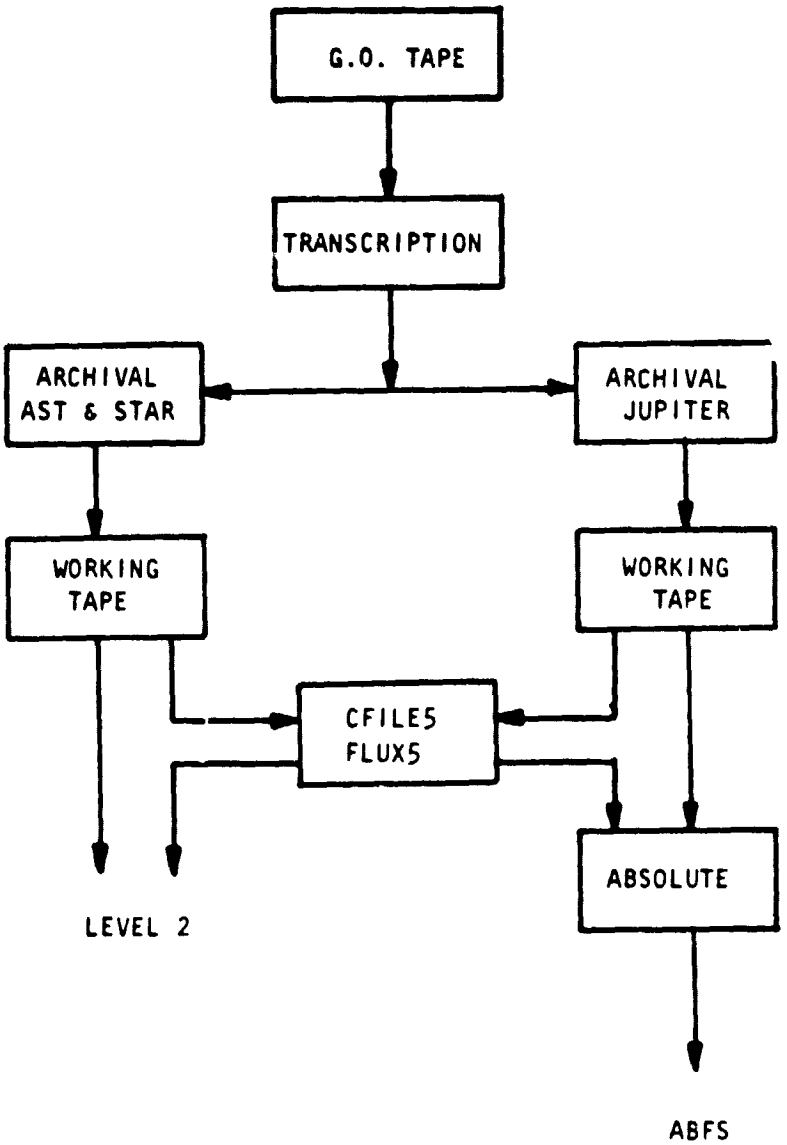

Fig. 1 LEVEL 1 PROCESSING

normalizes out the exposure time yielding a spectra on an absolute scale of ergs/(CM^2 -sec-Å). An additional working tape of the Jupiter file 5 spectra converted to an absolute scale, tape ABF5, was created for level 2 processing. For each image, the wavelength data and the absolute flux was stored over the wavelength range of the instrumental response function with the saturated reseaux contaminated, and negative flux pixels set to zero.

The major interest in the asteroid and star data images is wide-band photometry in the near ultraviolet. Program ASTS2 was the principle routine used in the processing of these images to accomplish this goal. The three main functions of routine ASTS2 were to: 1) apply the IUE Absolute Instrumental Response Function, 2) average the spectra, and 3) smooth and reaverage the spectra. After a spectrum was converted to the absolute scale, limited in wavelength range by the presence of usable data or existence of the response function, the data were averaged in 50A blocks. The spectra were then smoothed with a running 30Å rectangular filt (11 pixel wide) and then averaged in 50Å blocks. The output consists of the absolute and convolved spectra, the 50Å block averages and the standard deviations of the average values. The zero flux data were not averaged or convolved.

The second level of Jupiter processing was intended to generate data sets and image files of uniform length, format, spectral band coverage, and wavelength scale to facilitate all subsequent examination. This was necessary, if for no other reason, because of the shear amount (55 images) of data. With this goal in mind, the length of each spectrum was set at 152 pixels. Pixels 1-128 cover the wavelength band 1976.1--2537.8 Å, while pixels 129-152 cover the range 3237.5 - 3339.4 Å. The short and long wavelength cutoffs were determined by the S/N ratio (S/N>5) while the middle wavelength region was unusable due to saturation. The uniform wavelength scale was formed by the average of 35 wavelength scales from usable images 6055 - 6132.

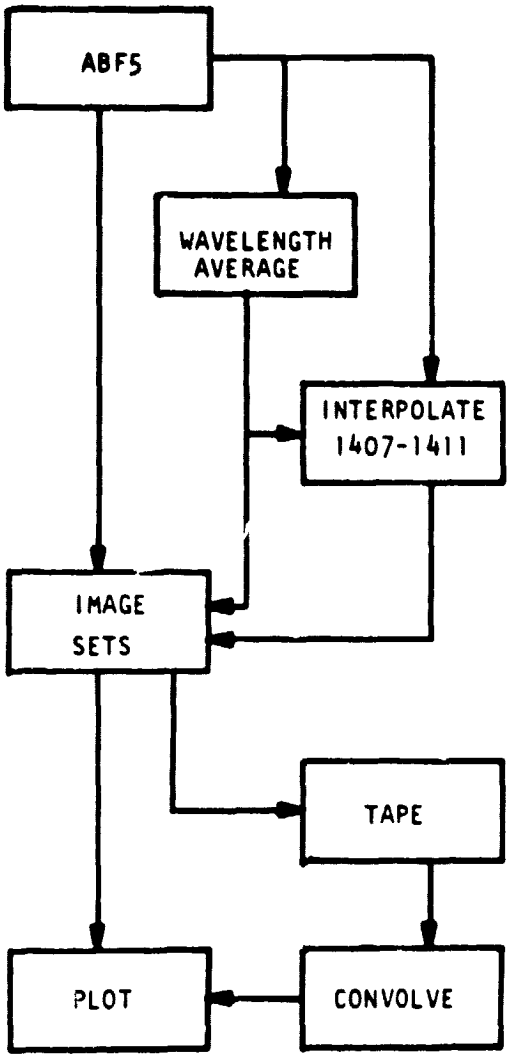

Fig. 2 LEVEL 2 PROCESSING

Care was taken to ensure that the spectral features overlapped and that differences in wavelength scales (typically less than 1 Å) were due only to systematic shifts of the whole scale. This was not the case with the earlier set of images 1407 - 1411. This data was interpolated with respect to the new wavelength scale in order to achieve consistency of format. Finally the spectral data were grouped into sets of data corresponding to specific limb-limb scans and stored on tape. This tape was then the source of data for ploting and smoothing. Some rsults are discussed in the next section. Figure 2 is a block diagram of the processing at this level.

C. Qualitative Description of Sample Data

Figure 3 shows a series of raw spectra from the center to the limb of Jupiter at equatorial latitudes. The noise in the spectra is evident. Figure 4 shows the same data after smoothing in wavelength with a 30 Å wide filter to reduce the noise. The spectra show a clear trend indicating limb brightening at all wavelengths in this interval. Indeed, the increase in brightness from the disk-center to the limb spectrum is ~ 15%. While this might appear to be a small amount of brightening, it should be noted that the limb spectrum was recorded at some 88% of the radius away from the center of the planetary disk where the incident sunlight per unit surface area of the planet is roughly half the value at disk center. A uniformly diffusing cloud deck would appear half as bright at this location as at disk center.

Three spectra (image numbers 6069, 6079 and 6074) from a second equatorial West-to-East series of spectra are shown in Figs. 5 and 6 on an absolute scale. The portion of the spectrum from about 2550-3230 Å is saturated and not displayed for these 4-minute exposures. In this series, the limb spectra are again comparable in brightness with spectra obtained near the center of the disk. A 30 Å wide average near 2500 Å from each of the 13 spectra which make up this scan is shown in Fig. 7. The location of the limb and the amount of limb-brightening in the data are readily apparent. The data from both equatorial center-to-limb

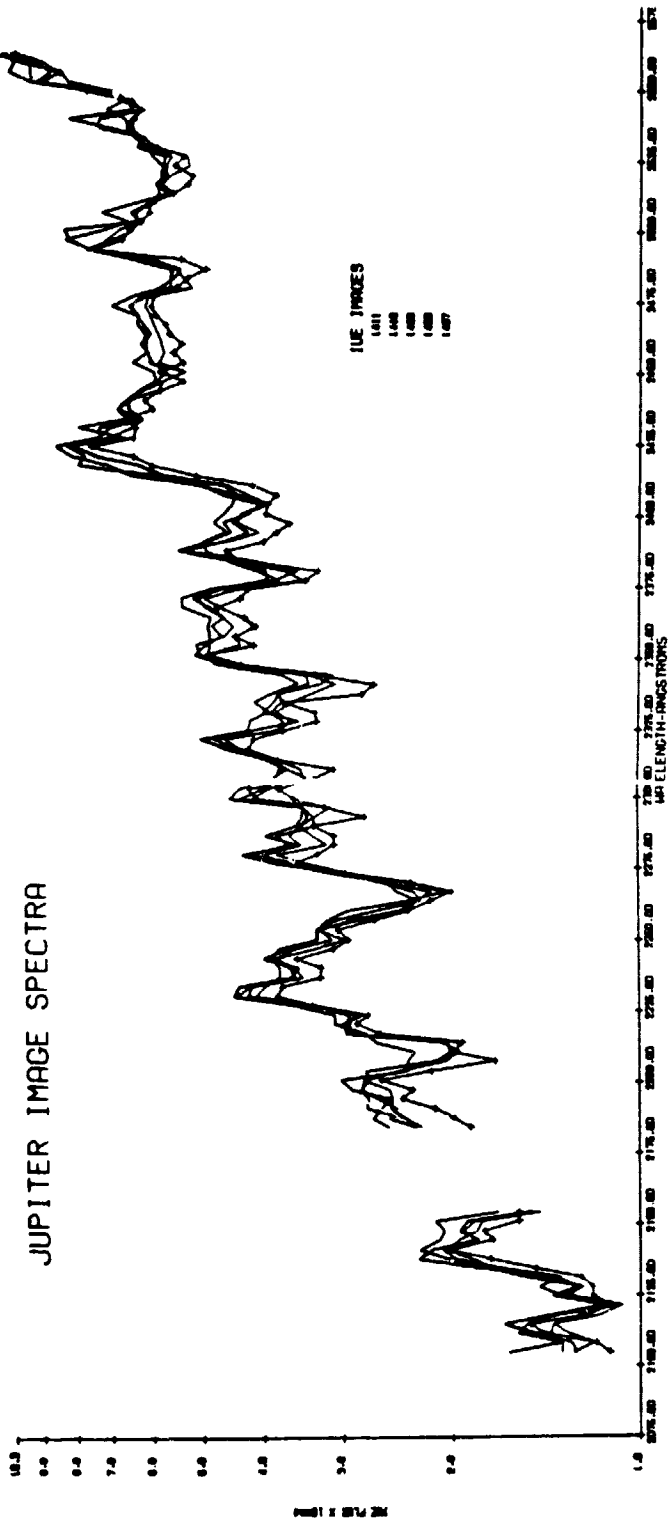

Fig. 3. Raw spectra of the equatorial region of Jupiter from images 1407 (near the center of the disk) to 1411 (near the limb).

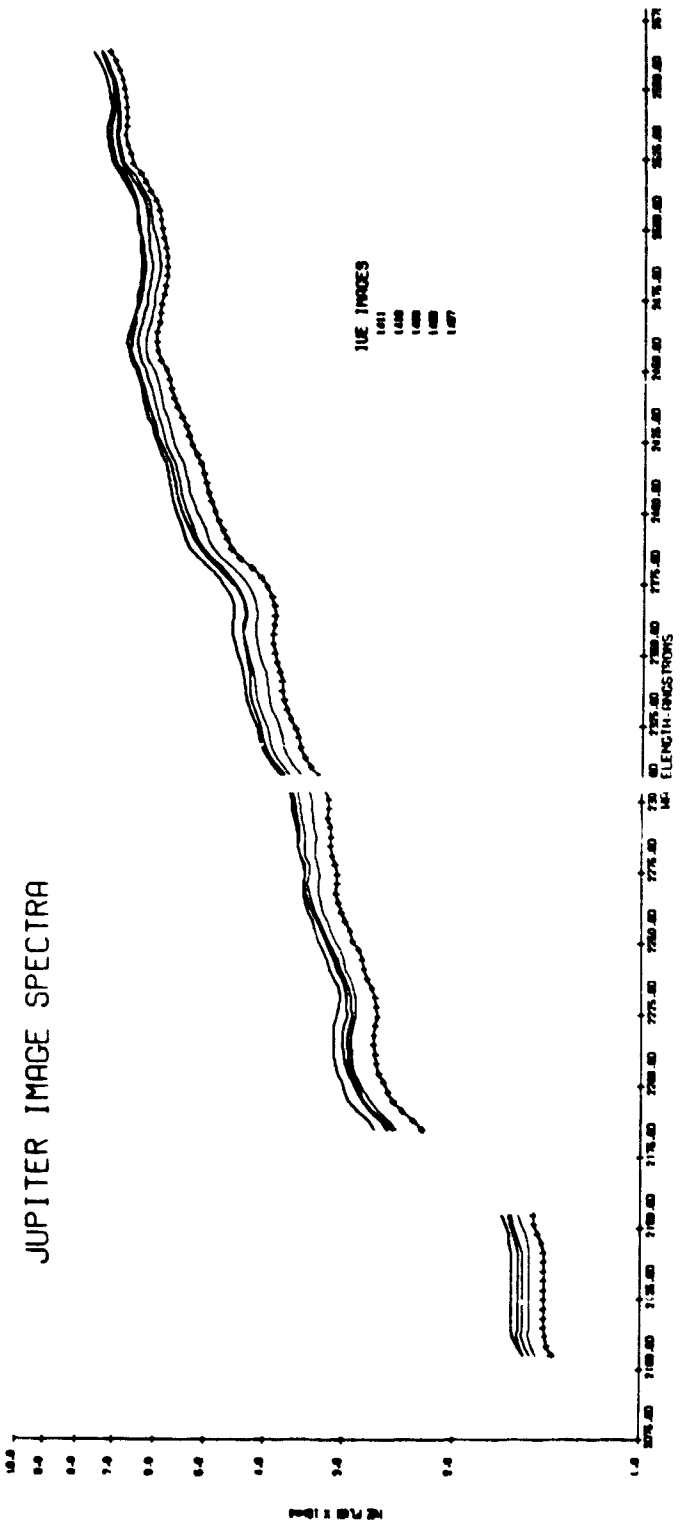

Fig. 4. Same as Fig. 3, but after smoothing in wavelength to reduce the noise. The general increase in brightness from image 1407 (disk center) to image 1411 (limb) is apparent.

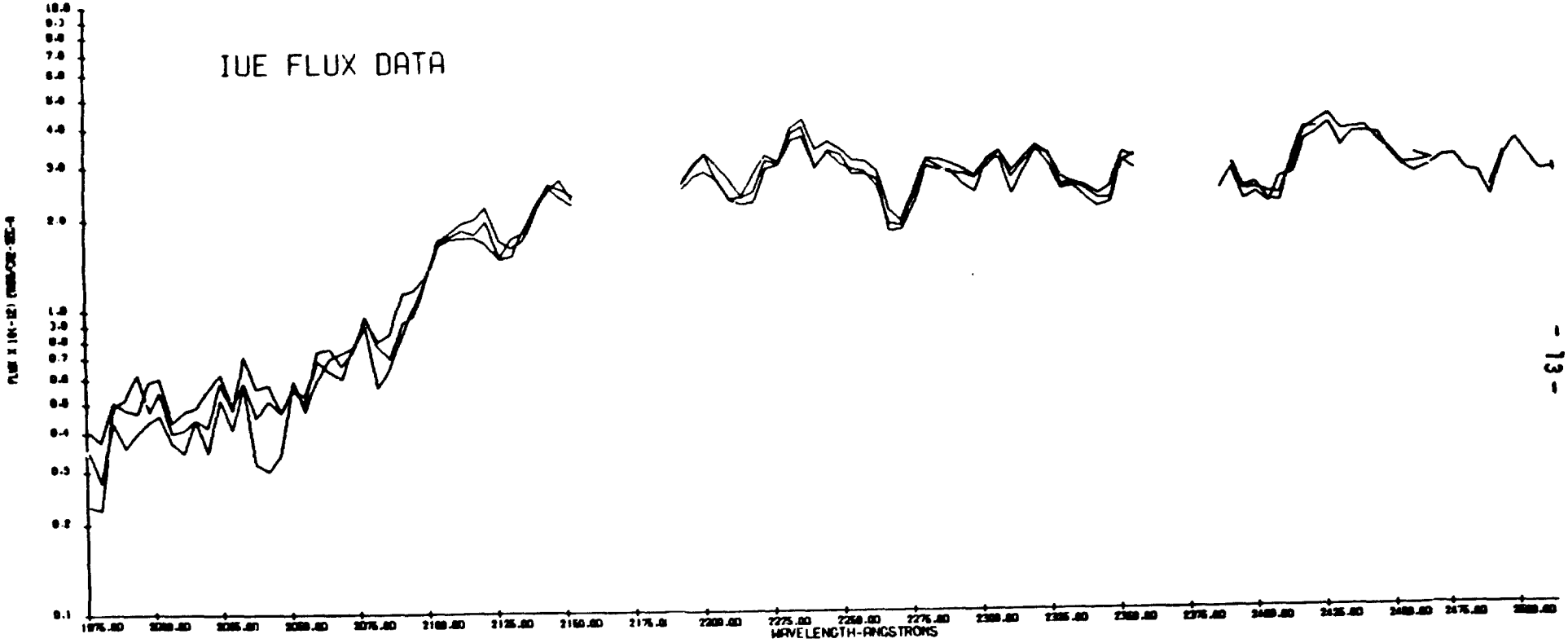

Fig. 5. Spectra of the equatorial region of Jupiter from images 6069, 6074 and 6079 converted to an absolute scale of ergs/cm^2-sec$\mathring{A}$ in the small (nominally 3 arc second diameter) aperture.

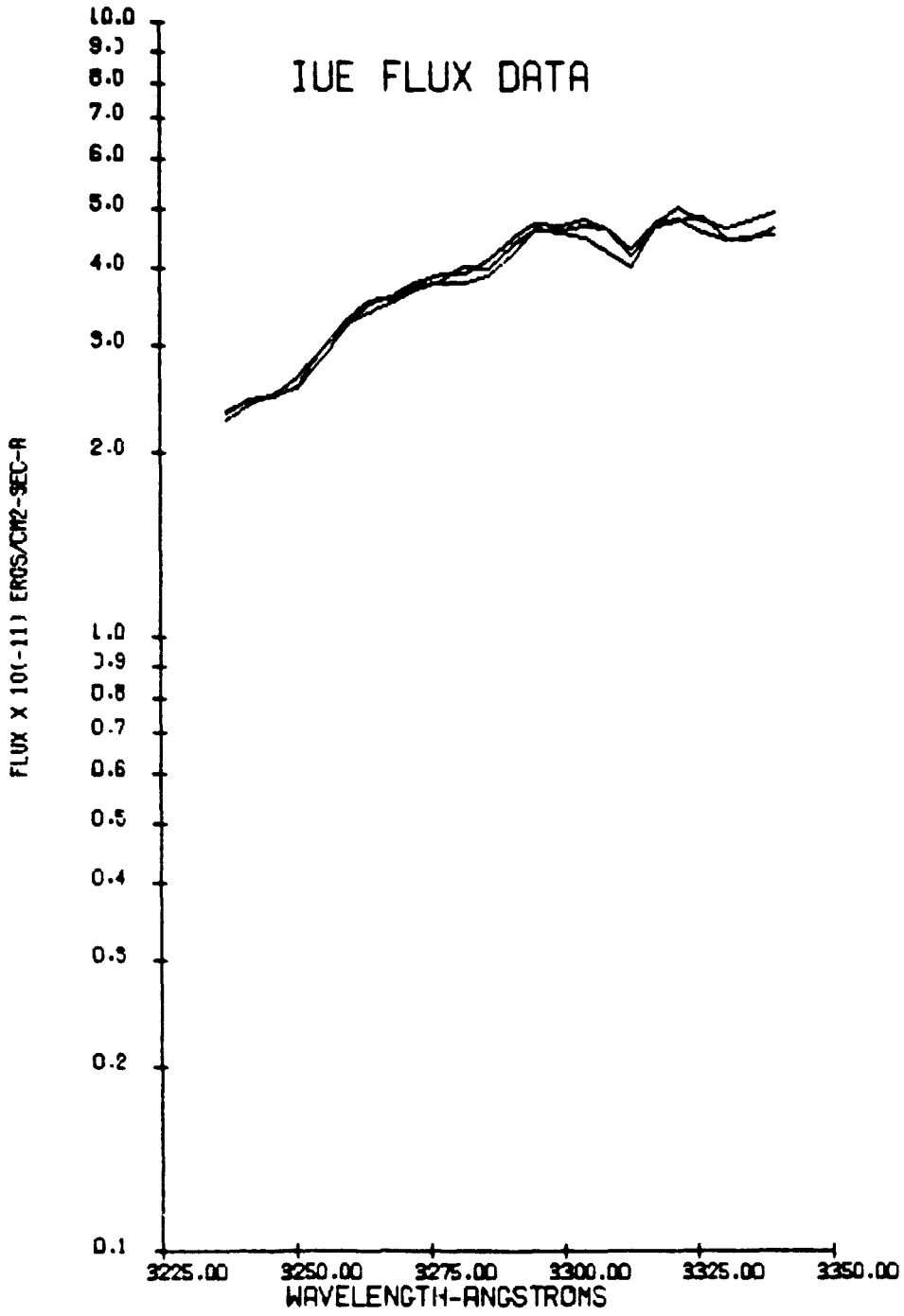

Fig. 6. Same as Fig. 5, but for the unsaturated long wavelenth end of the spectrum.

series indicate the presence of a relatively clear layer of hydrogen gas several km-amagats thick above the absorbing aerosols (see section IV below).

Figure 8 shows 30 Å wide averages of brightness at 4 wavelenths from a North-South series of spectra. The spectra plotted at 45 degree latitude are entirely on the planet. The polar regions are seen to be much darker (by a factor of at least 3) at these wavelengths than the center of the disk. This result is consistent with the observations at 2400 Å by the Viking 2 photopolarimeter reported by Hord et al. in Science, 206, 956, 1979. These data indicate that the absorbing aerosols must be mixed to significantly higher levels of the atmosphere at latitudes greater than about 30 degrees.

If this is the case, the amount of limb brightening in East-West scans at high latitudes should be significantly less than that observed at low latitudes. Figure 9 shows data at 4 wavelengths from an East-West scan at 45 degrees North latitude. The data at 2500Å can be directly compared with the equatorial limb scan shown at the same wavelength in Fig. 7. In contrast with the situation at low latitudes, the high latitude scan shows definite limb darkening, even after allowance is made for the relatively greater smearing due to the 3 arcsecond aperture. The increased limb darkening observed at high latitudes is qualitatively as expected for aerosols extending to higher altitudes at high latitude.

It is also interesting to note from Figs. 8 and 9 that while the planet is brighter at 2200Å than at 2500 Å at the center of the disk, the opposite is true at 45 degrees latitude. If the absorbing aerosols are quite small, as has been suggested, they can become more important at shorter wavelengths. However, the Rayleigh scattering of the clear gas also increases very rapidly with decreasing wavelength. It may be that only when the gas abundance above the aerosols is considerably reduced, as at high latitudes, can the aerosols dominate the gas and give decreasing

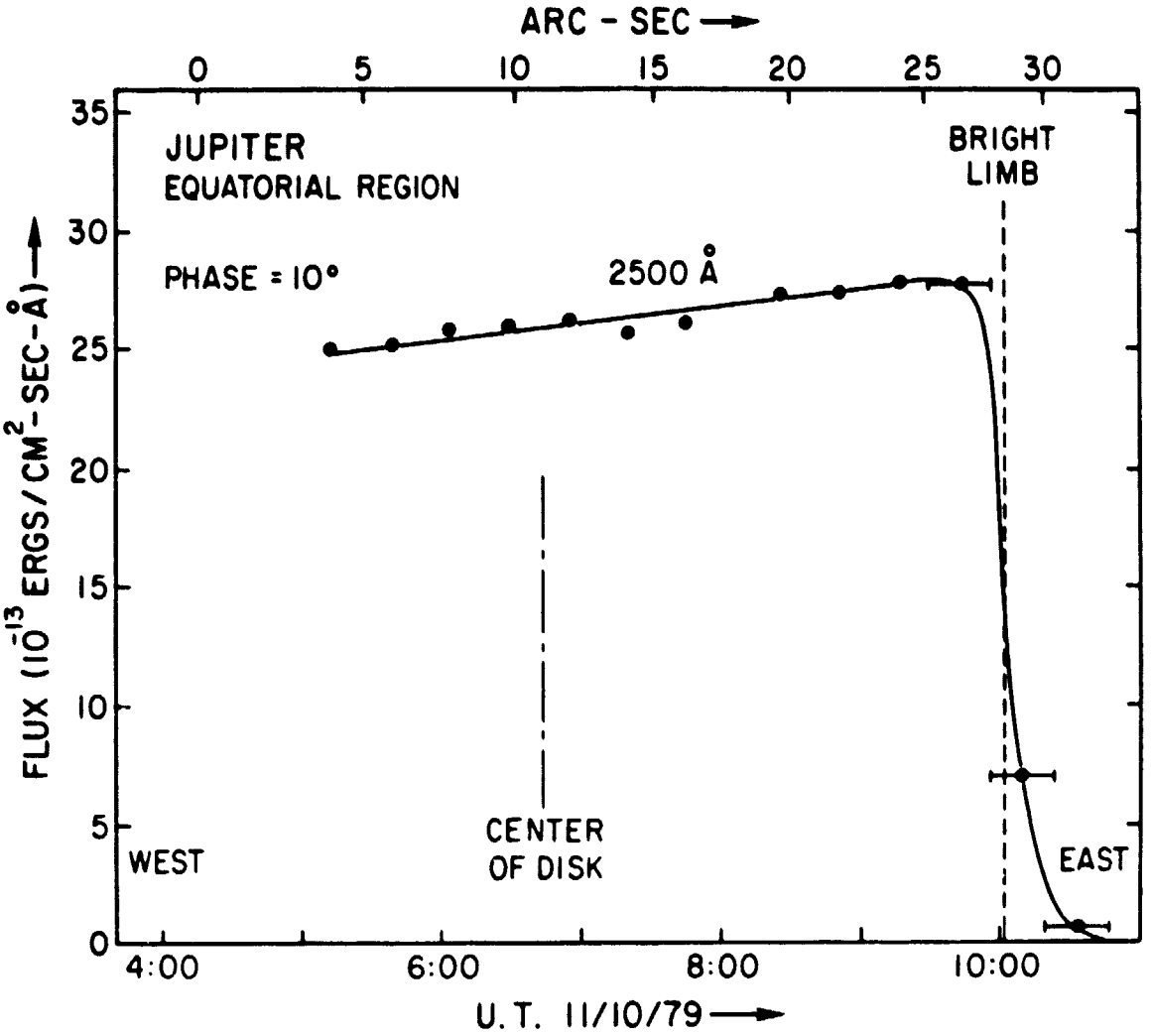

Fig. 7. Average flux observed in the small aperture for a 30Å wide portion of the spectrum near 2500Å in spectra 6069-6081 plotted vs time the spectra were taken. Tracking on the satellite Ganymede was used to move the aperture across the disk in the equatorial region. The position of the limb, disk center, and the size of the 3 arc-second aperture are indicated.

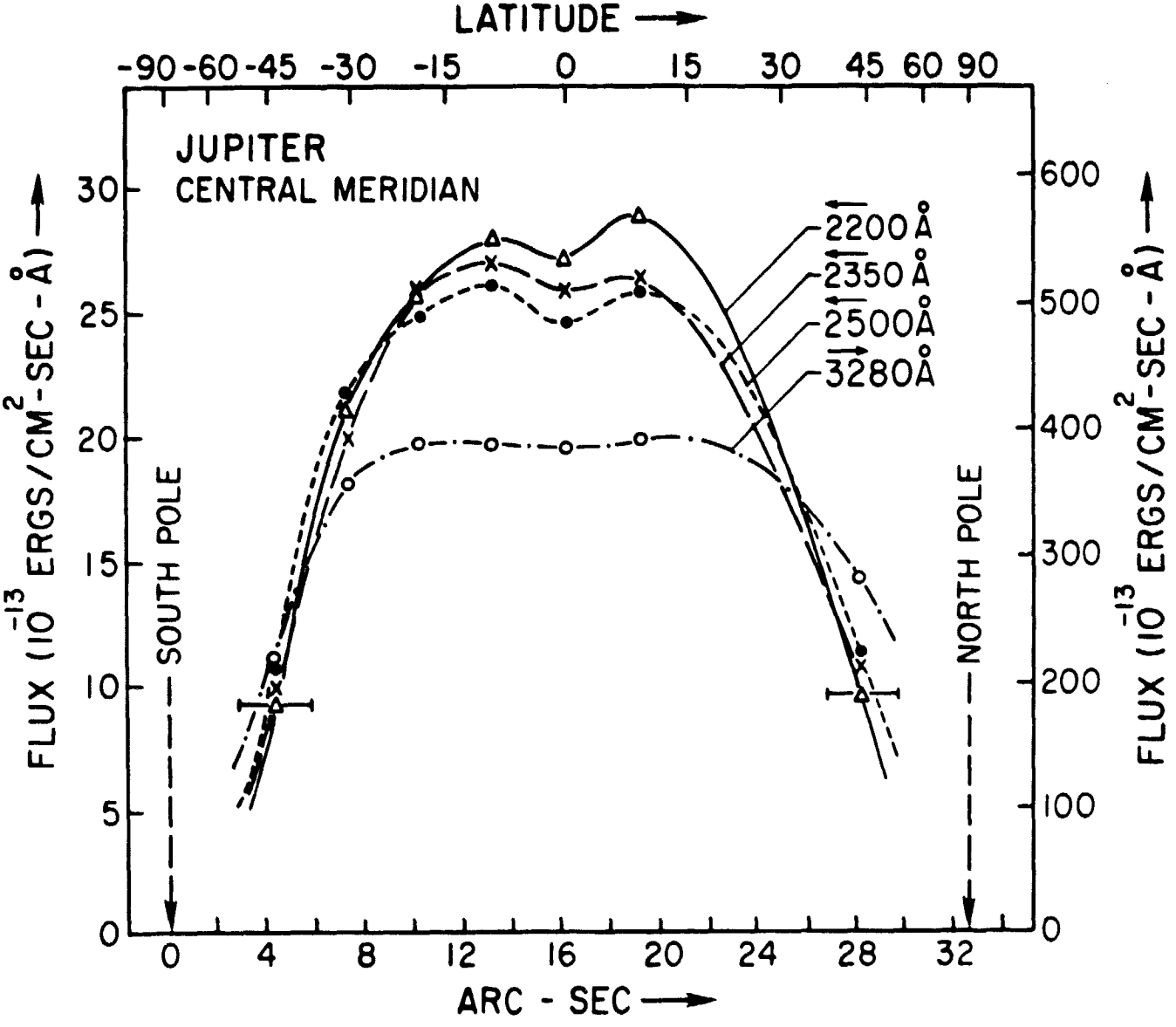

Fig. 8. Similar to Fig. 7, but for four wavelengths as labeled in a South-North series of spectra along the central meridian. Successive offsets from Ganymede were used to position the aperture.

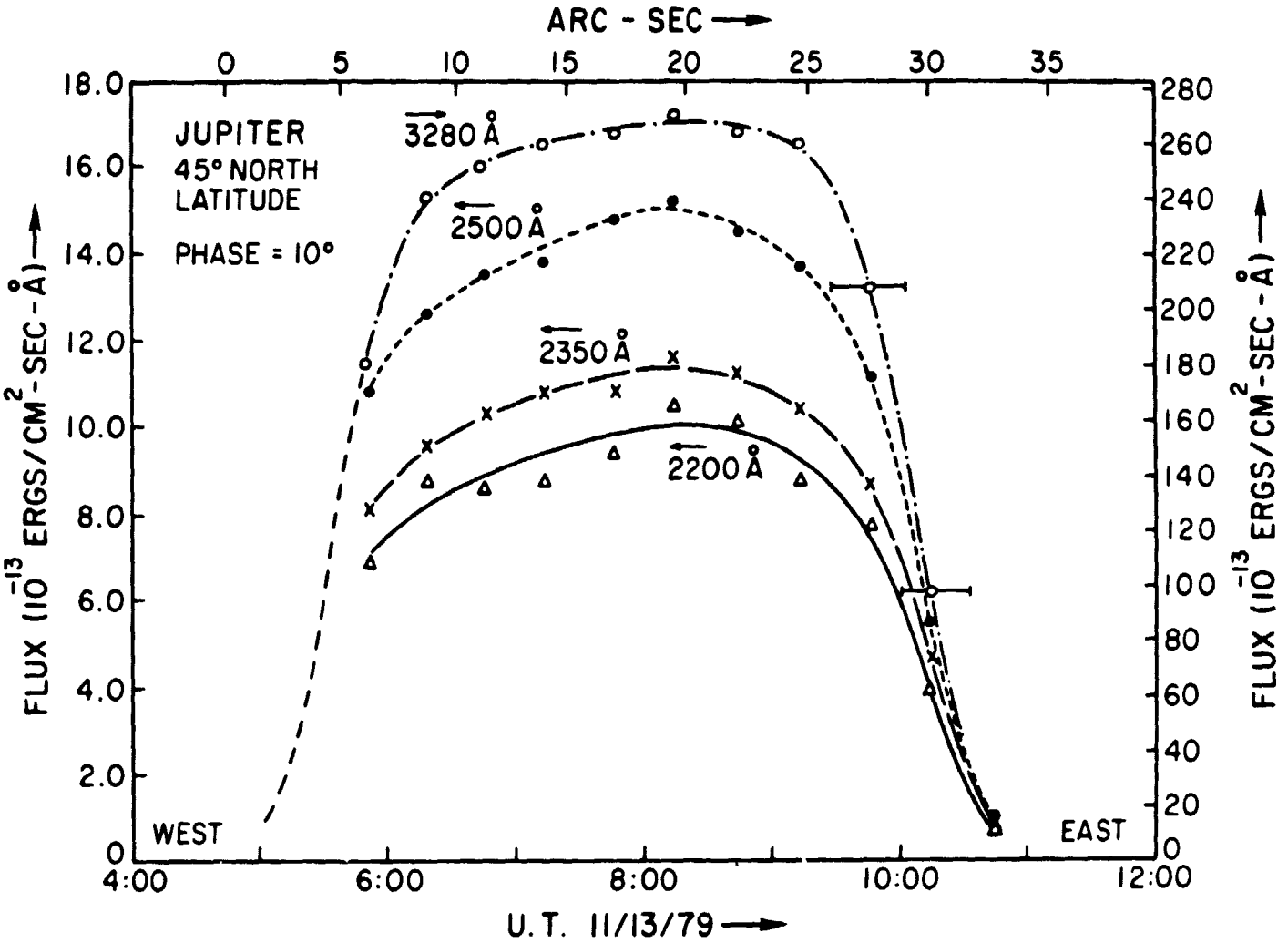

Fig. 9. Similar to Fig. 7. but for a West-East scan at 45° North latitude. The plotted points are from image numbers 6123 to 6133. Tracking on Callisto was used to move the aperture across the disk.

brightness with decreasing wavelength.

In any case,this series of IUE spectra of Jupiter has successfully shown several important types of brightness variation over Jupiter's disk in the ultraviolet: limb brightening at low latitudes, a strong decrease in brightness toward the poles, limb darkening at high latitudes, and the spectral variations of each. A comparison of these observations with model calculations is in progress, and some detailed results for the limb brightened scans at low latitudes are presented in section IV.

At this writing most of the data reduction for the asteroids and for the solar-type stars is still in progress. All of the data have been examined, saturated or underexposed pixels rejected, and the remainder averaged in 50 Å bins. Figure 10 illustrates the results for the solar-type star HD 10800, composited from four images of varying exposure.

Figure 11 illustrates ratio spectra, normalized by the above data for HD 10800, for the S-type asteroids 3 Juno and 27 Euterpe, the C-type object 1 Ceres, and the unclassifiable object 4 Vesta. The two S asteroids show a definite family resemblance. The spectrum of Ceres is also similar, but that of Vesta rather different, and a spectrum of the M object 16 Psyche is strikingly different. We hasten to add that these results are highly preliminary and should not be taken literally. In particular the fine spectral structure may be genuine but more likely results from imperfect reduction to the spectrum of the Sun.

IV. JUPITER MODELING RESULTS

A. Special Processing to Extract Limb Darkening

Images 1407 - 1411 form the first sequence of equatorial center-to-limb observations and their limb brightening characteristics have been investigated most extensively. In a

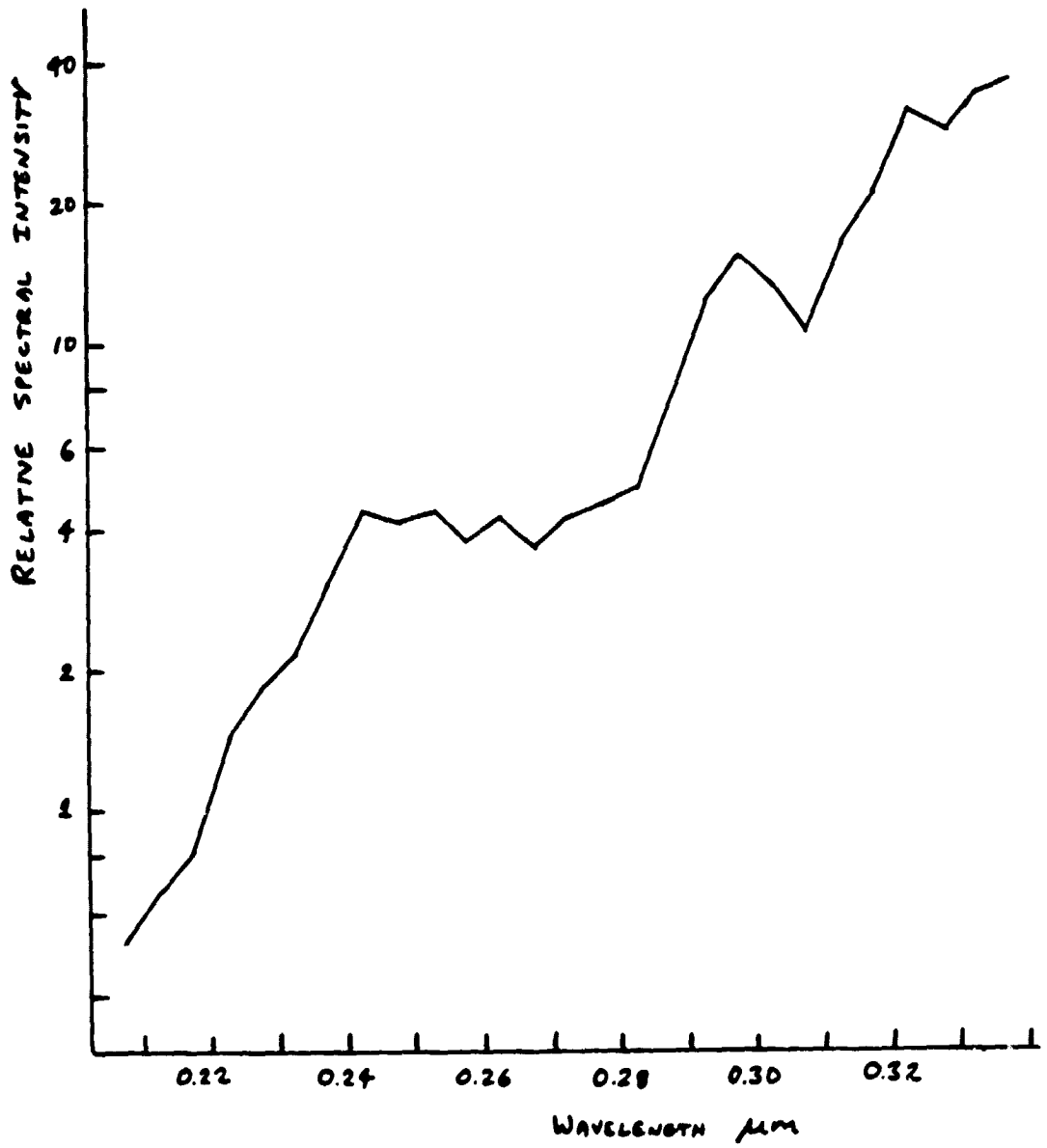

Fig. 10. Relative spectral intensity of the solar-type star HD 10800, composited from four spectra on LWC 6088 and 6089. Data are averaged in 50Å bins.

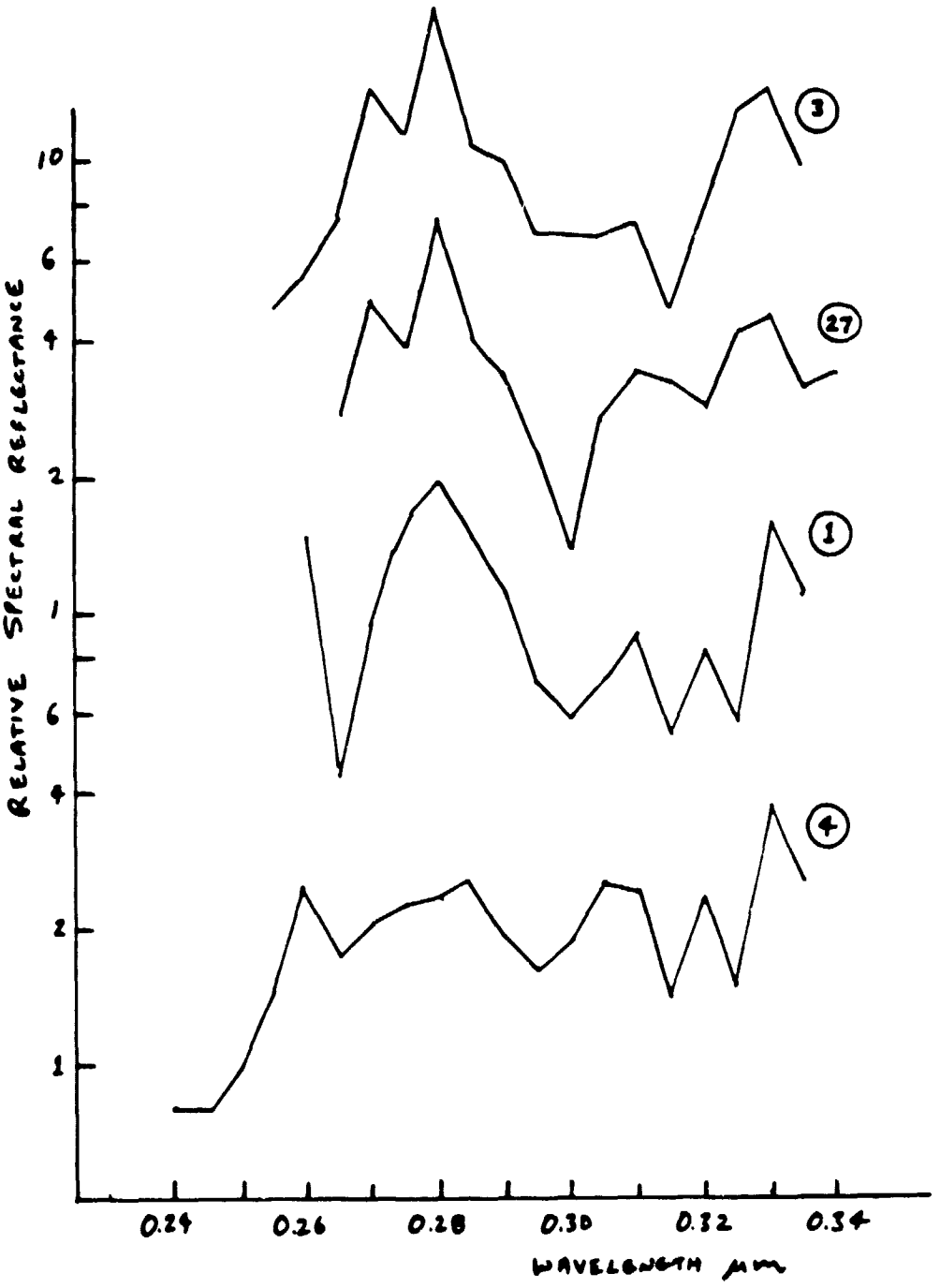

Fig. 11. Relative spectral reflectance of minor planets 3 Juno, 27 Euterpe, 1 Ceres, and 4 Vesta, from preliminary reductions using HD 10800 as a solar analogue. Data are averaged in 50Å bins.

plot of 1407 and 1411 the systematic increase of irradiance with limb position is evident, however, in a plot of all the spectra, as in Fig. 3, random signal fluctuations are obvious. In fact, the short term reproducability (hours) of IUE spectra is 2-3% (1sigma) uncertain averaged in 600Å wide spectral bands (see "Photometric Calibration of the IUE," NASA X-681-79-19, June, 1979, Table 6.). Direct pixel-by-pixel ratioing of spectra was inadequate to determine the brightening in the presence of these fluctuations.

A special technique was devised to obtain the best estimate of the amount of limb brightening as a function of wavelength in the presence of noisy spectral data. The processing steps in determining the brightening function are illustrated in Fig. 12. The first step is to smooth the data in wavelength by convolution with a 25 pixel wide filter. A typical result of this process was shown in Fig. 4.

The second step is to fit a function relating brightness to radius at each wavelength. Model investigations indicated (and Fig. 7 shows) that for the case of data having only small (10-20 percent) brightness variations with radius, the brightness varies nearly linearly with increasing distance from the center of the disk.

Accordingly, a routine (SLOPE) was written to perform a weighted least-square straight-line fit of the IUE FN versus normalized limb position at each wavelength.

$$I_{\lambda,i} = A_\lambda + B_\lambda (R_i/R_J) = A_\lambda + B_\lambda r_i$$

where R_i: radial limb position of image

R_J: radius of Jupiter

B_λ: slope of limb brightening as a function of wavelength

A_λ: Convolved spectra at planet center

The equation is transformed by dividing by A, such that

$$I_\lambda/A_\lambda = I'_\lambda = 1 + (B_\lambda/A_\lambda) r_i = 1 + B'_\lambda r_i$$

where $100 \times B'_\lambda$ is effectively the percent brightening at the limb. The standard deviation of B'_λ was also computed.

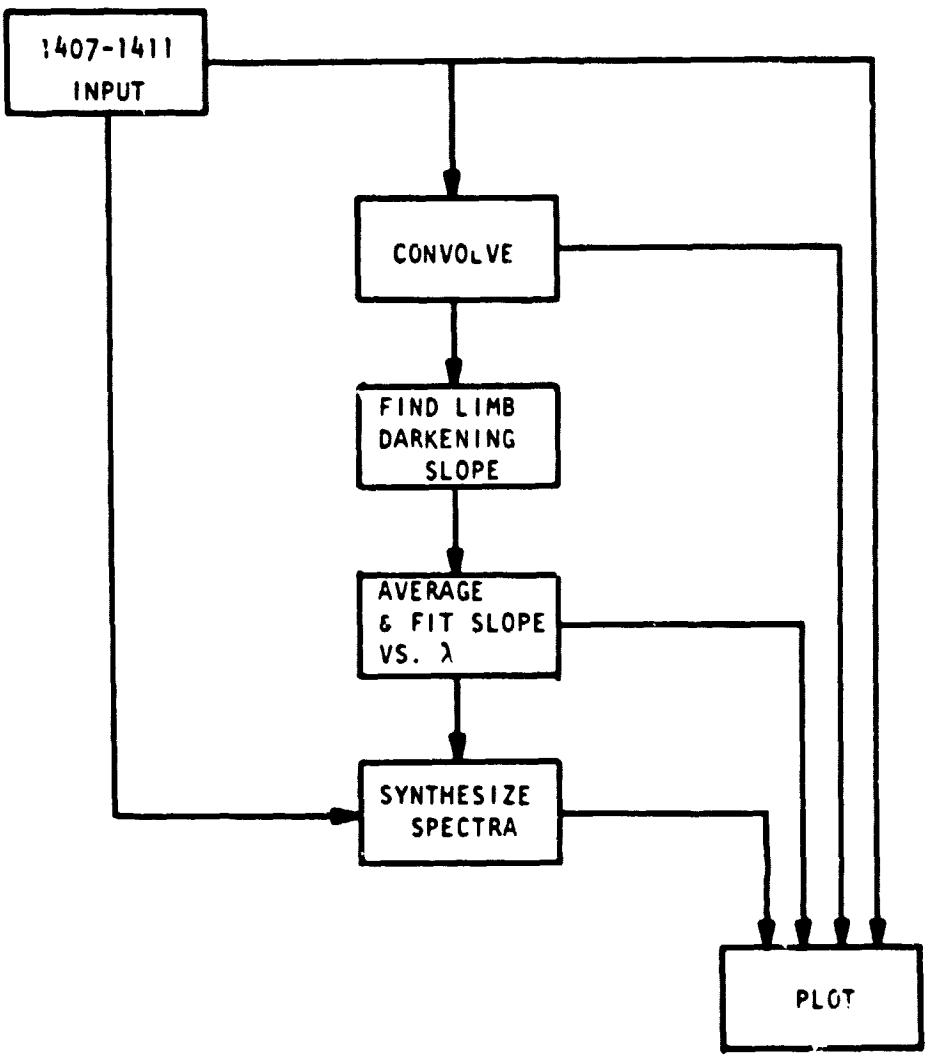

Fig. 12 LEVEL 3 JUPITER PROCESSING

In order to further reduce the uncertainty of the computed slope values, B'_λ, they were averaged in 0.01 increments of optical depth, τ. Where τ per km-am of H_2, for a 77.57% H_2, 22.43% He mixture is given by

$$\tau = \frac{2.311 \times 10^{-4}}{\lambda^4} + \frac{3.43 \times 10^{-6}}{\lambda^6} + \frac{1.285 \times 10^{-8}}{\lambda^8}$$

(wavelength in microns).

The resulting twelve data points and standard deviations were incorporated in a least-square parabolic fit. The parabola and the data points are displayed in Fig. 13. The best fit equation for the slope as a function of τ is:

$$SLP(\tau) = B' = -0.186337 + 5.81163\tau - 23.3353\tau^2$$

Finally, the function for the brightening slope as a function of optical depth can be utilized to minimize and quantify the random error of the input spectra. The slope function was used to remove the brightening due to limb position, and hence reduce the unconvolved spectra to the planet center. The five spectra were then averaged and the standard deviation of the mean computed. At a given value of τ (or wavelength):

$$I_c(\tau,i) = I_{raw}(\tau,i)/(1 + SLP(\tau)\, r_i)$$

where i is the image number index, such that

$$\bar{I}_c(\tau) = 1/5 \sum_i I_c(\tau,i)$$

and

$$\sigma^2 = 1/5 \sum_i (I_c(\tau,i) - \bar{I}_c)^2$$

The value of $\sigma(\tau)$ ranged from 1% to 3%, within the uncertainty of repeatability over short time periods reported by the IUE staff observers.

Finally, the slope function was applied to synthesize the image spectra using the computed mean spectra for the planet center:

$$I_i(\tau) = \bar{I}_c\ (1 + SLP(\tau) r_i)$$

The result is plotted in Fig. 14. Deviations of these synthesized spectra from the raw spectra were computer printer plotted. No systematic trends were detected suggesting that the errors in the input spectra were indeed random.

Therefore, given the limitation imposed by assuming a

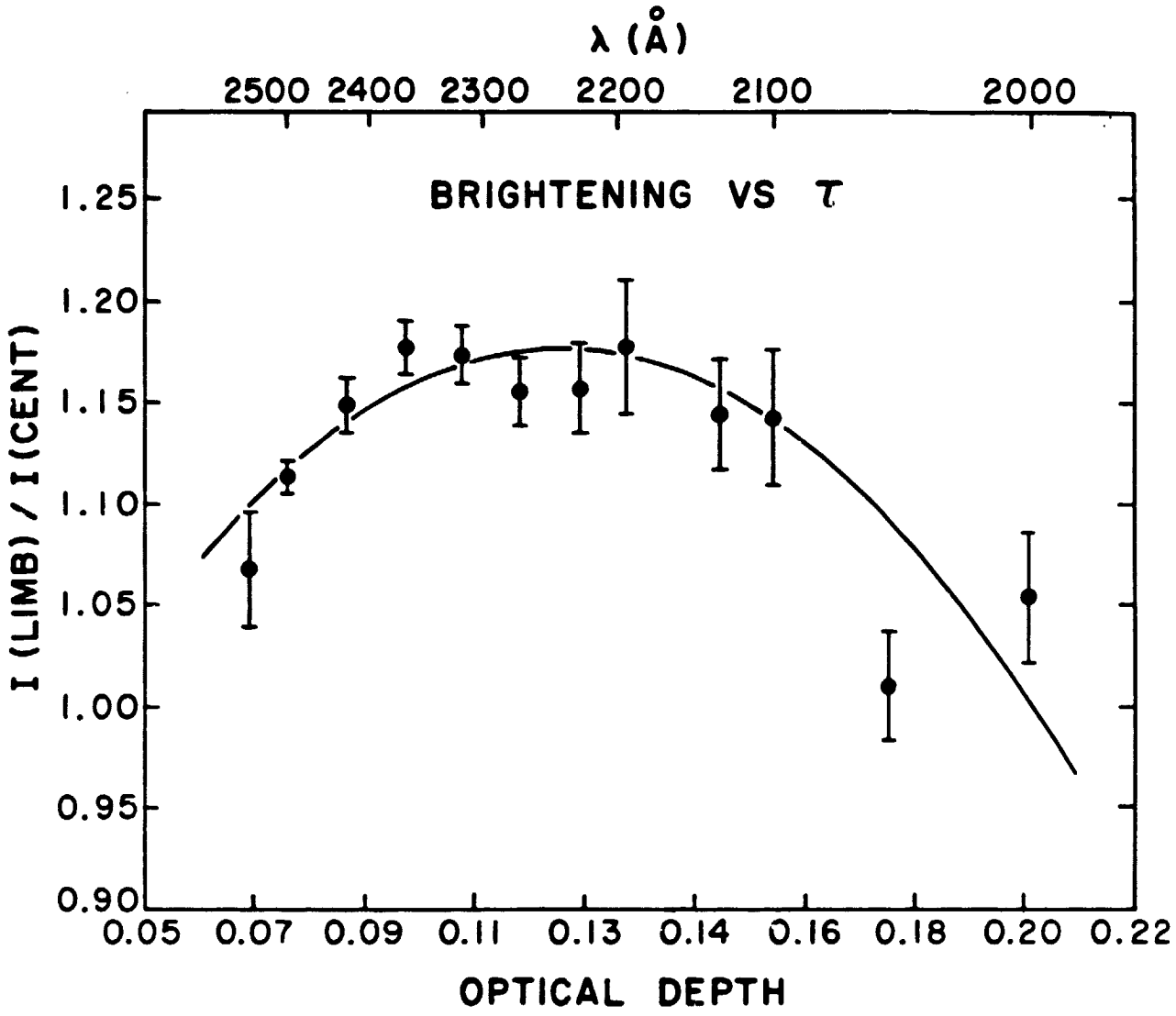

Fig. 13. Ratio of limb to disk center brightness for the equatorial region on Jupiter from an analysis of images 1407 to 1411 plotted against wavelength (top scale) The wavelength scale is stretched to make it linear in Rayleigh scattering optical depth (bottom scale). The two points shortward of 2080Å are from spectra 3409-3413.

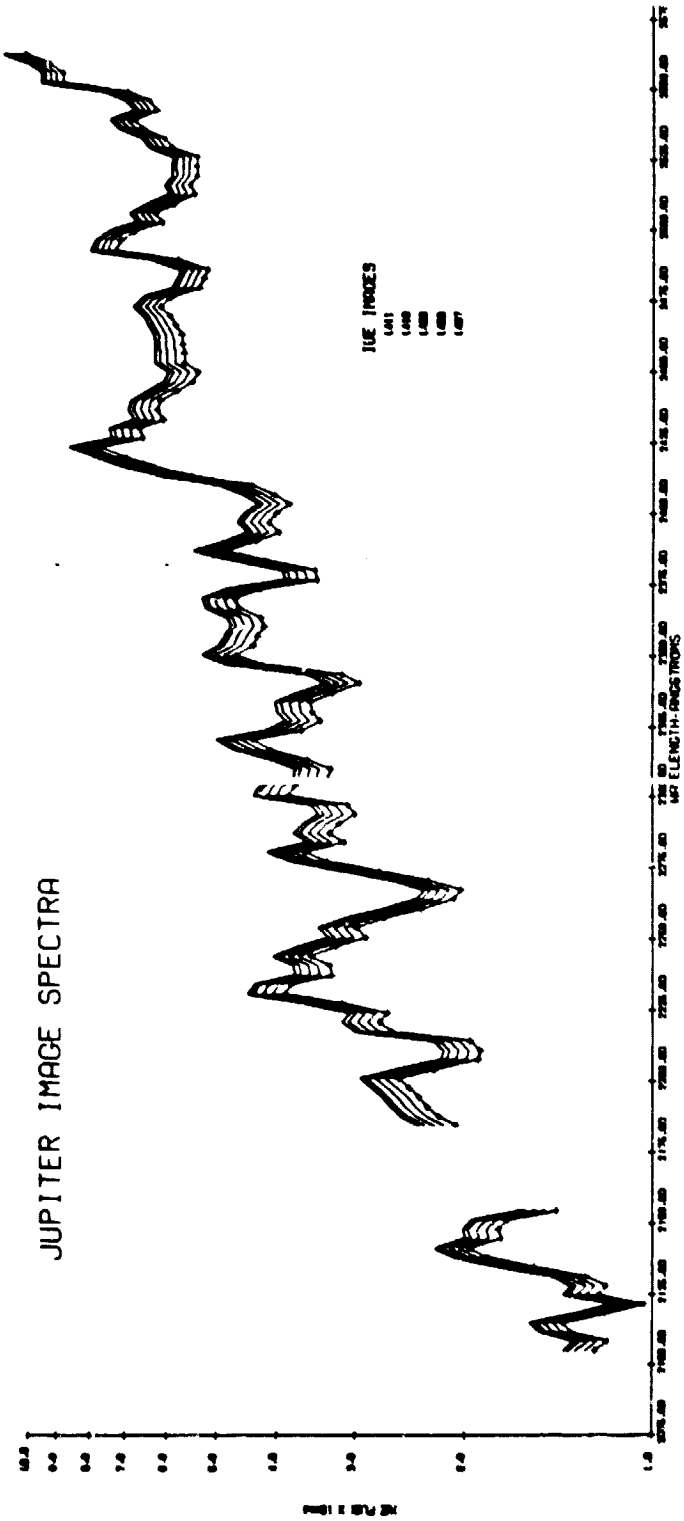

Fig. 14. Synthesized version of spectra 1407 to 1411 produced by modeling the wavelength dependence of the limb darkening by the parabola shown in Fig. 13 as described in the text.

brightening function linear with limb position, it was possible to obtain an expression for the brightening as a function of wavelength (or optical depth) and to remove the random errors present in the spectral features to within the uncertainty present in the repeatability of the instrument.

B. Model Results for Equatorial Spectra 1407 - 1411

The wavelength dependence of the limb-darkening was determined by the above technique from images 1407 - 1411. Figure 15 shows the intensity computed at these locations on the disk at wavelengths of 2200Å and 2500Å. The model consisted of various abundances of clean, Rayleigh scattering gas above a thick haze (optical depth = 8). Below the thick haze are another 12 km-amagats of clean hydrogen, and then the ammonia cloud deck. The single scattering albedo of the haze was adjusted to give about the correct geometric albedo of the model for each run. The layers beneath the haze remained very bright in this calculation, but at a haze thickness of 8, they affected the model only very slightly. Figure 15 indicates that for this structure, the data imply that the abundance of clean gas above the haze must decrease from about 5-6 km-amagats at 2500Å to 3-4 km-amagats at 2200Å. Such an effect is qualitatively possible if the aerosols are quite small and if their size decreases with height in the atmosphere. In this case, the smallest aerosols near the top of the model can have a much greater optical depth at shorter wavelengths, causing the apparent cloudtop to move up in the atmosphere with decreasing wavelength.

Figure 16 shows a measure of the limb-darkening observed plotted against wavelengths. Also shown are contours of the limb brightening that is produced by various abundances of clear gas above the thick haze. Again, the decrease in gas abundance to shorter wavelengths is apparent. Notice that 5-6 km-amagats of clean hydrogen above the haze fits the data reasonably well from 2500Å down to 2350Å. At still shorter wavelengths, the model must be modified by raising the top of the haze, or by other means.

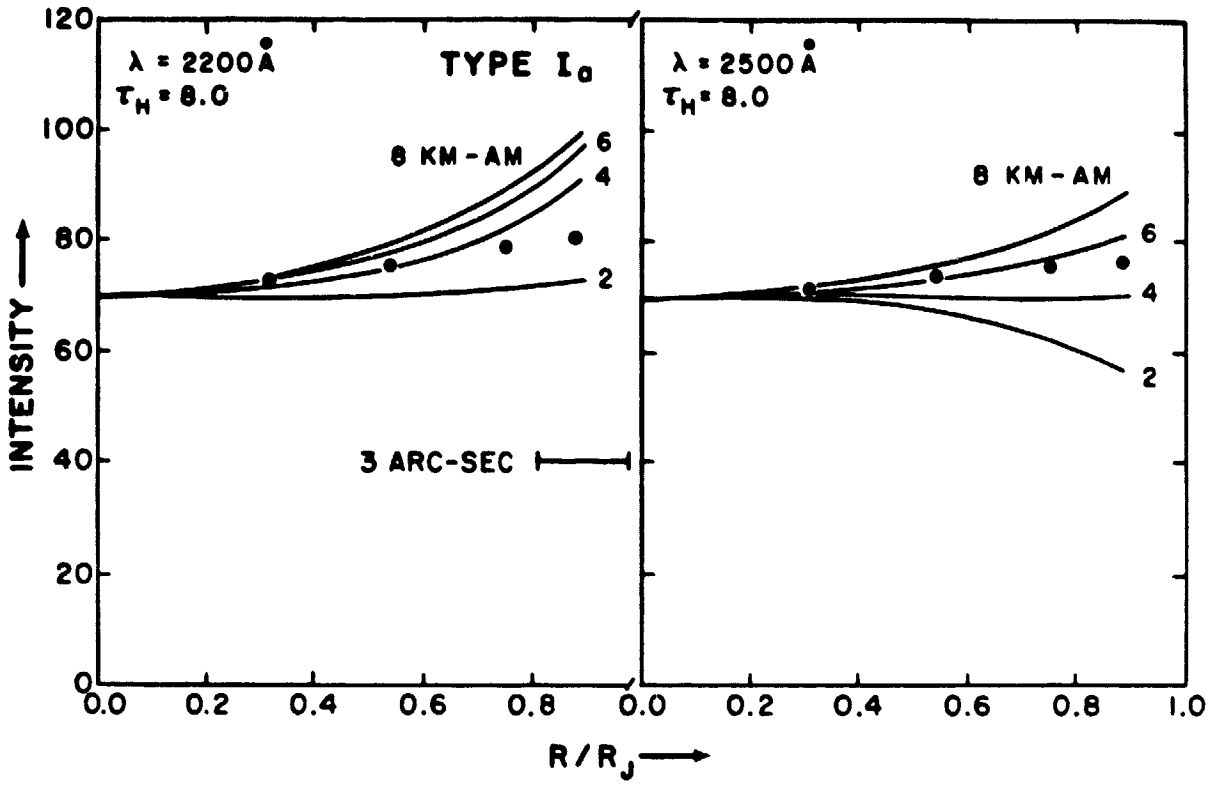

Fig. 15. Computed limb darkening curves (lines) compared with data from images 1407 to 1411 (dots) at wavelengths of 2200Å and at 2500Å. The curves are for various abundances of clean hydrogen gas above an absorbing haze of optical thickness equal to 8. See text for other details of model structure.

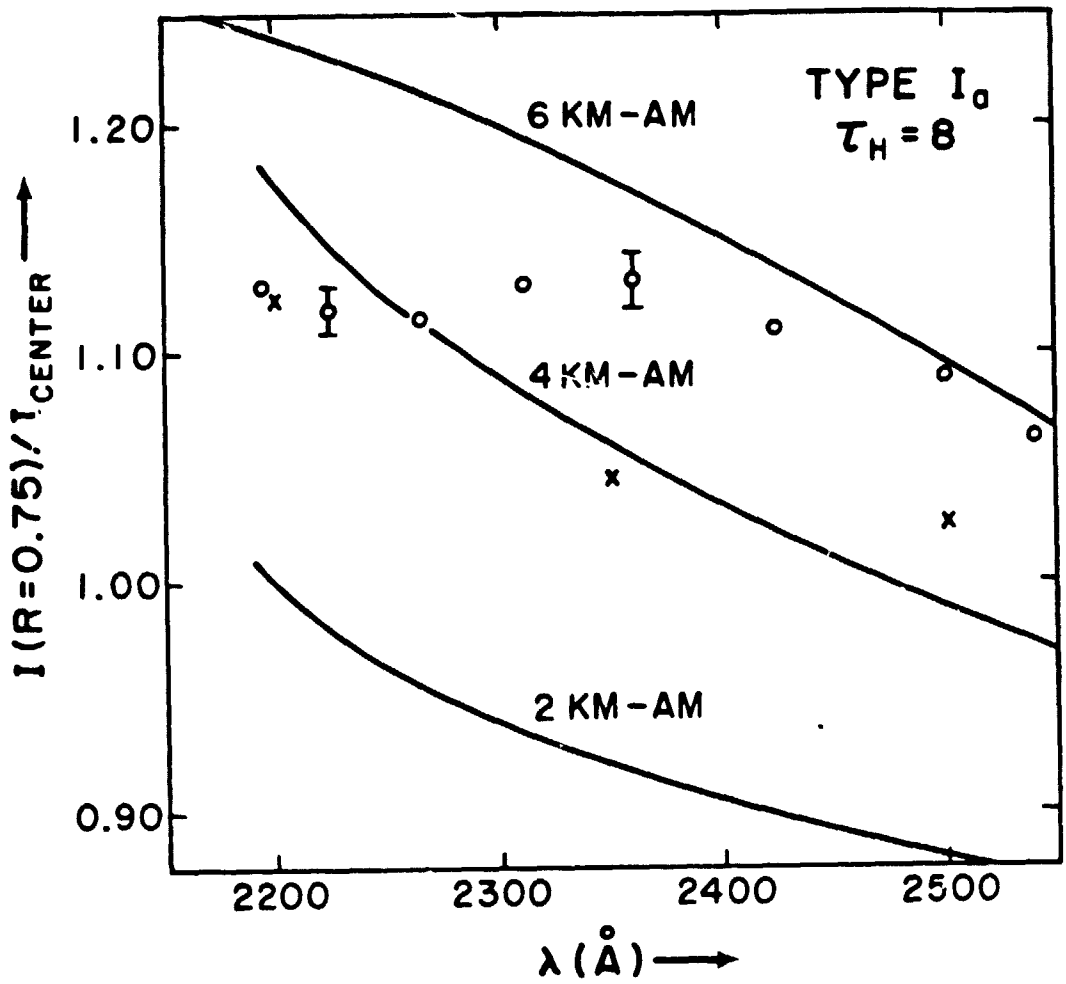

Fig. 16. Fractional increase in brightness at 3/4 of the planetary radius from the center relative to the brightness at the center of the disk plotted against wavelength. The points are from the analysis of images 1407 to 1411. The curves show the wavelength dependence of the model described in the text for various abundances of clean hydrogen gas above an absorbing haze of optical thickness 8.

A variety of data (see Tomasko, M.G., R. West, and N.D. Castillo, Icarus, 33, 558, 1978 and West, R.A. and M. G.Tomasko, Icarus, 41, 278, 1980) suggests that the haze above the ammonia cloud deck has an optical depth (at equatorial latitudes) of only a few tenths in the visible. In order to explore models of this type, we allowed the cloud representing the ammonia particles to have the same single scattering albedo as the haze. This single scattering albedo was determined by requiring the geometric albedo at each wavelength to match the values observed by OAO (see L. Wallace, J. J.Caldwell, and B.D. Savage, Ap.J. 172, 755, 1972. Figure 17 illustrates that at 2500Å, the observed limb brightening is not especially sensitive to the haze optical depth in the range from 0.5 - 1.0. The required gas abundance above the haze in this case is between 6 and 8 km-amagats. Figure 18 demonstrates that for haze thickness = 0.5, about 7 km-amagats above the thin haze fits the limb-darkening at 2350Å as well as at 2500Å.

Figure 19 shows the locus of values of haze thickness and hydrogen abundance above the haze for limb-darkening fits at 2200, 23250, and 2500Å. Again, notice that the data at 2200Å requires the haze to extend to somewhat higher levels.

Recall that absorption only occurs in the model in the haze layer and in the NH_3 cloud found beneath an additional 12 km-amgats of clean hydrogen. This means that even if the single-scattering albedo of the haze and cloud particles are set to zero, there is a minimum achievable geometric albedo for the model which depends on the haze thickness. Thus, at 2500Å, the haze must have an optical thickness of at least 0.5, and at 2200Å, at least 1. This increase in optical thickness from 0.5 at 2350Å to 1 at 2200Å is accompanied by the top of the haze appearing to extend to higher altitudes at the shorter wavelengths.

These preliminary modeling studies of a portion of this IUE

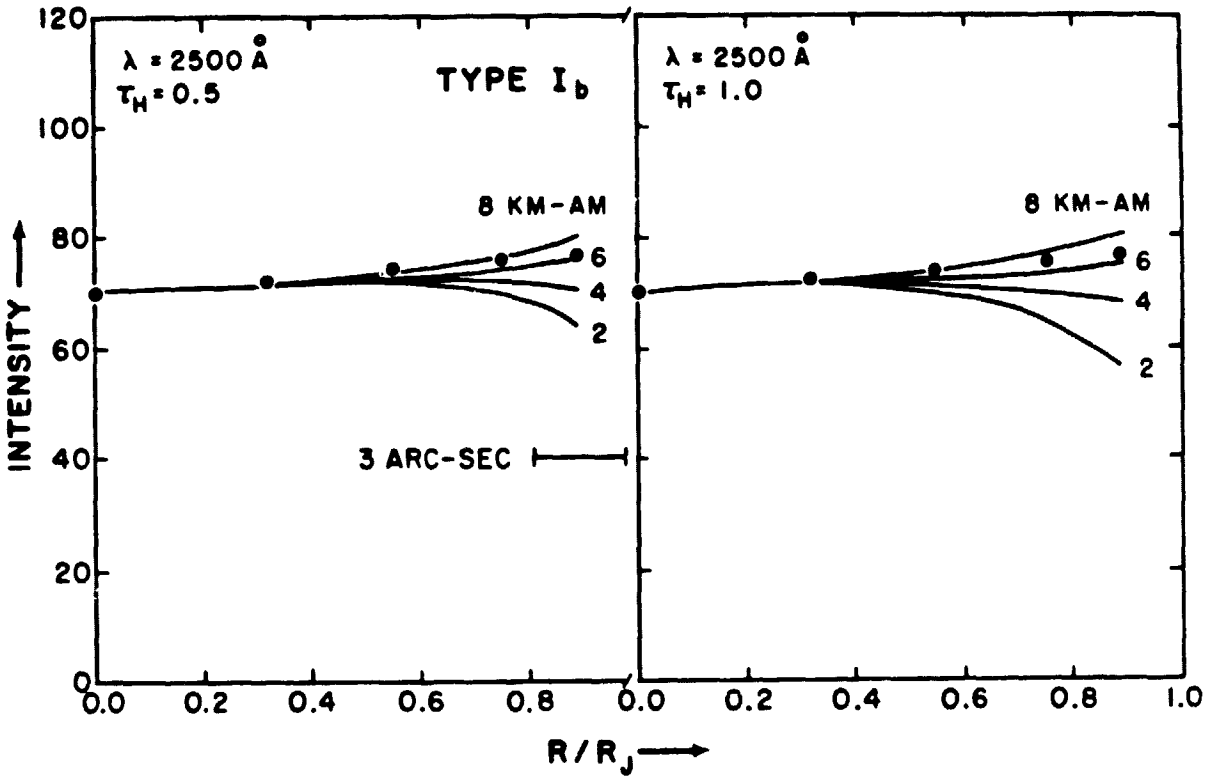

Fig. 17. Similar to Fig. 15, but for haze thicknesses of 0.5 and 1.0 at 2500Å. Beneath the haze are 12km-amagats of clean hydrogren followed by a thick cloud of particles having the same single scattering albedo as those in the thin haze.

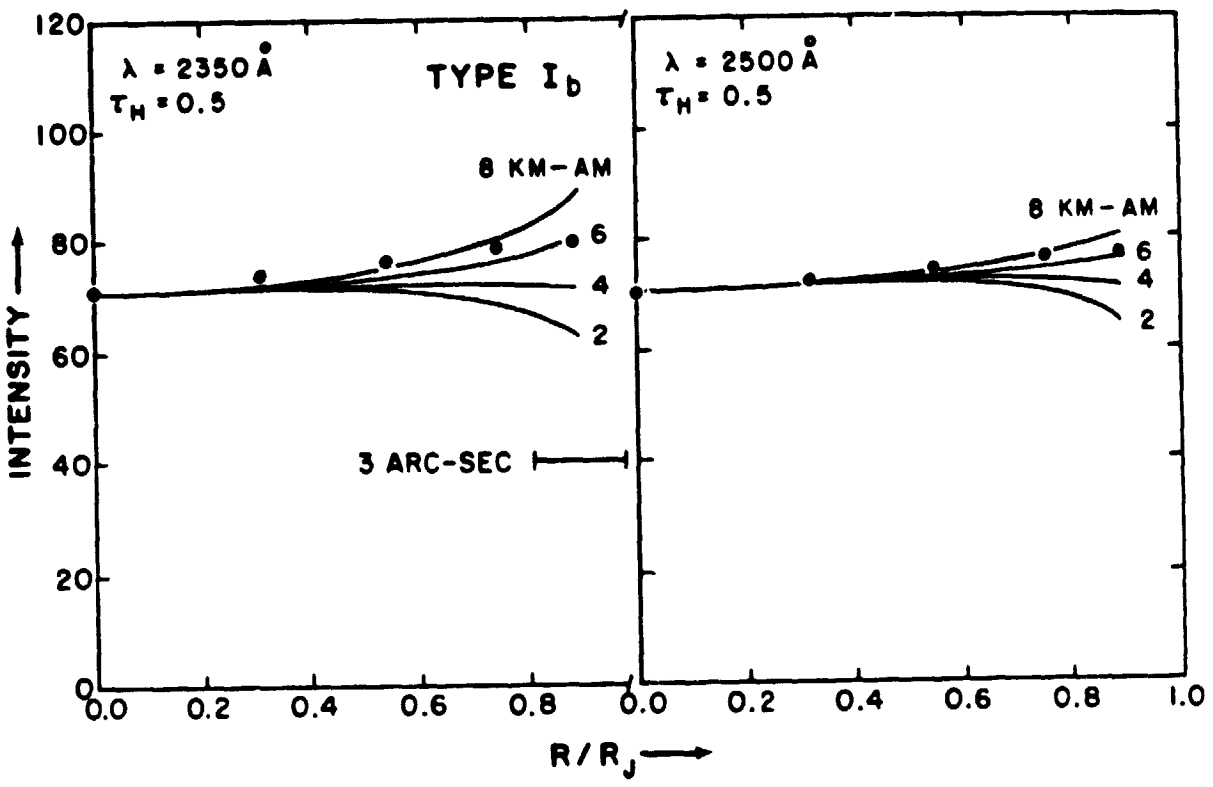

Fig. 18. Same as Fig. 17 but at 2350 and 2500Å at a haze thickness of 0.5. Note that 6 to 8 km - amagats of hydrogen above the haze give a reasonable fit at both wavelengths.

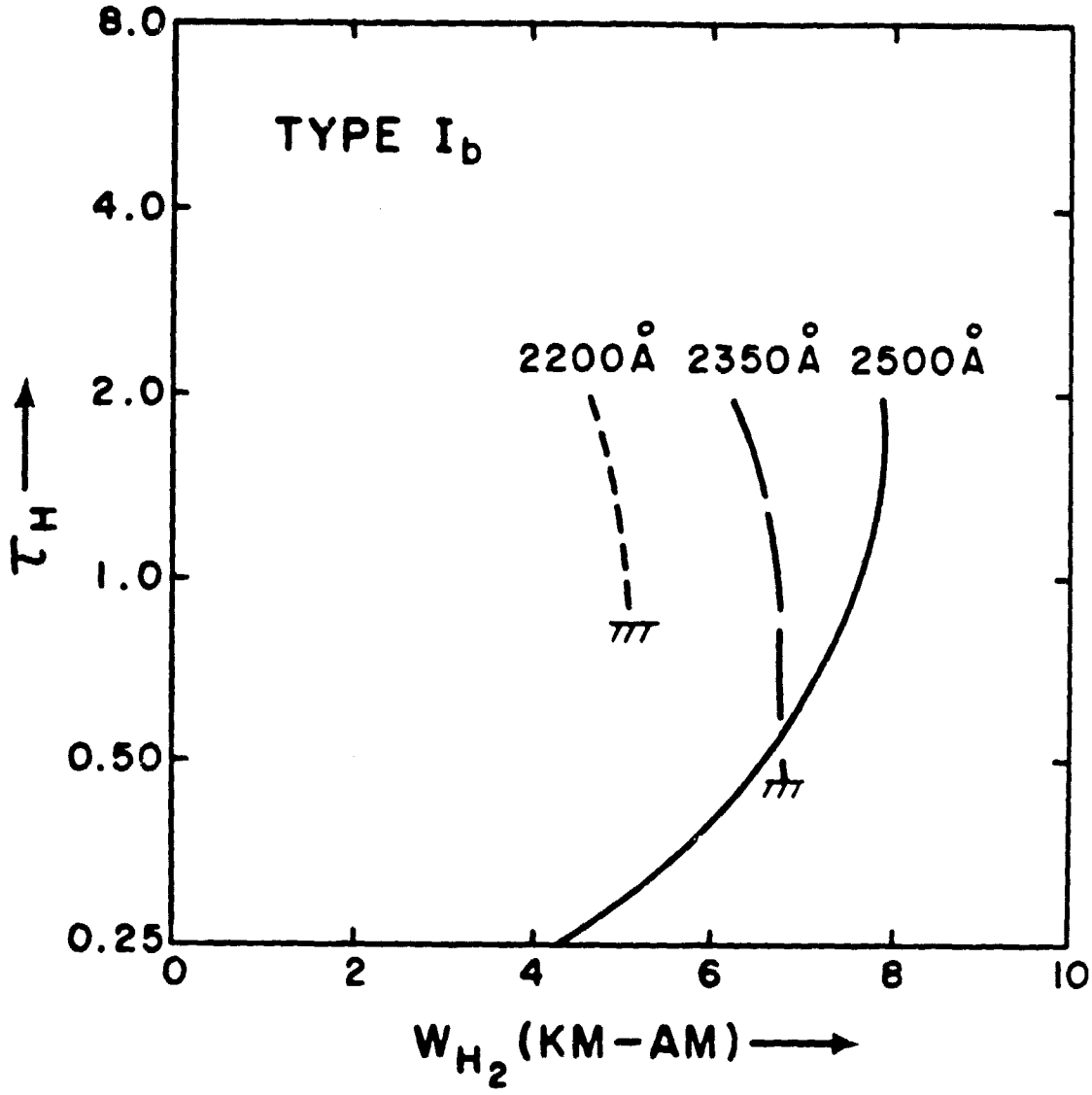

Fig. 19. Locus of values of haze thickness and gas abundance above the haze which fit the equatorial limb-brightening observed in images 1407 to 1411 at 2200Å, 2350Å, and 2500Å. At 2200Å the haze can not be thinner than about $\tau=1$ and at 2350Å the haze can not be thinner than about $\tau=\frac{1}{2}$ without making the planet brighter than is observed at these wavelenths.

data set have been reported in the following:

"Ultraviolet observations of planets and satellites: First results from IUE", M.G. Tomasko, XXI Meeting of COSPAR, Innsbruck, Austria, 1978.

"The distribution and optical properties of aerosols in the upper atmospheres of Jupiter", M.G. Tomasko, XXI Meeting of COSPAR, Innsbruck, Austria, 1978.

"Center-to-limb variations in the ultraviolet spectrum of Jupiter", M. G. Tomasko and S. Martinek, Bull. of Amer. Astron. Soc. 10, 562, 1978.

"Observations of solar system objects with the International Ultraviolet Explorer", A. L. Lane, T. C. Owen, M.G. Tomasko, H.W.Moos, G. E. Hunt, C.A. Barth, R. Conway, T. Gehrels, T. R. Gull, and E. H. Hamrick, Bull. of Amer. Astron. Soc. 10, 587, 1978.

"Observations of solar system objects with the International Ultraviolet Explorer", A. L. Lane, A. Boggess, D. C. Evans, T. R. Gull, T. C. Owen, H. W. Moos, M. G. Tomasko, T. Gehrels, G. E. Hunt, R. Conway, C. A. Barth, F. Schiffer, B. Turnrose, P. Perry, A. Holm, F. Macchetto, E. Hamrick, Nature, 275, 414, 1978.

"Center-to-limb variations in the ultraviolet spectrum of Jupiter measured by the International Ultraviolet Explorer Satellite",M. G.Tomasko, Session of COSPAR Meeting Concerning Planetary Observations from Earth-Orbiting Vehicles, held June, 1980, in Budapest, Hungary.

We are currently involved in extending these models, applying them to our other East-West and North-South scans, and comparing their constraints on the Jovain haze with that of other ground-based and spacecraft observations we have acquired with other support. We plan to publish our detailed results upon the completion of our modeling studies.